Hydrodynamic Experimental Investigation On Efficient Swimming of Robotic Fish Using Self-propelled Method

Article *in* International Journal of Offshore and Polar Engineering · September 2010

CITATIONS
22

READS
271

3 authors, including:

Li Wen
aasd
197 PUBLICATIONS **2,667** CITATIONS

SEE PROFILE

Guanhao Wu
Tsinghua University
81 PUBLICATIONS **586** CITATIONS

SEE PROFILE

International Journal of Offshore and Polar Engineering (ISSN 1053-5381)

Vol. 20, No. 3, September 2010, pp. 167–174

http://www.isope.org/publications

Hydrodynamic Experimental Investigation on Efficient Swimming of Robotic Fish Using Self-propelled Method

Li Wen and Jianhong Liang
Robotic Institute, School of Mechanical Engineering and Automation
Beihang University, Beijing, China

Guanhao Wu
State Key Laboratory of Precision Measurement Technology and Instruments
Department of Precision Instruments, Tsinghua University, Beijing, China

Jinlan Li
Department of Electrical and Computer Engineering, National University of Singapore, Singapore

Efficient swimming of biologically carangiform robotic fish has been investigated by using a novel experimental method. The laboratory robotic fish model, which follows an exact replica of Saithe, is self-propelled on a servo towing system. The forward towing speed is determined by the fluid force acting on the robotic fish, as the fish undulates its body in the water. The importance of the self-propelled method, which allows for simultaneous measurement of internal and external forces on the robotic fish, has been demonstrated in the hydrodynamic experiment. The hydrodynamic result shows that the optimal efficient swimming pattern of the robotic fish is found at a parametric value where Strouhal number (St) and body wave speed δ are proximal dimensionless parameters of live undulatory swimmers, a maximum drag reduction rate of 38% is recorded, and the drag-reduction is defined as P_f/D_uU, where P_f is the pure fluid power, D_u is the rigid drag force, and U denotes the self-propelled swimming speed.

INTRODUCTION

Through bionic engineering, the high thrust performance of fish is used to make up for the defects in traditional underwater vehicles, especially the low efficiency. In this paper, we choose to imitate the carangiform fish, which belongs to the BCF (Body/Caudal Fin propulsion) swim pattern (Sfakiotakis et al., 1999). The undulate swimming of the carangiform can be conceptualized as the action of 2 waving plates, one plate positioned in the other's wake (Muller et al., 1997, 2000, 2001). The tail corresponds to the downstream waving plate, while the body is the upstream waving plate; both plates will infer the thrust efficiency of the fish by combining two major flow mechanisms:

• Reasonable body waving to produce minimum drag (Taneda and Tomonari, 1974).

• Proper caudal fin movement to generate maximum thrust force according to vorticity control (Anderson and Chhabra, 2002; Barrett et al., 1999; Nauen and Lauder, 2002; Lauder and Drucker, 2002; Cheng, 1994; Lighthill, 1970).

Sufficient previous research provides evidence that the dimensionless parameters are closely related to efficient fish swimming (Triantafyllou et al., 2000; Taylor et al., 2003). When the vorticity mode of the fish swimming footprint, as it were, is too difficult to use for establishing its mathematical analytical equations or to obtain a dynamic model, hydrodynamic experiment analysis using dimensionless parameters becomes a powerful scientific solution (Hoerner, 1965). Reasonable dimensionless parameters will make swimming fish generate optimum vorticity distribution and intensity (Tytell and Lauder, 2004), which as a result gives higher swimming efficiency.

Several key dimensionless parameters are considered in our research:

• Strouhal number (Triantafyllou et al., 1993), which can be defined as:

$$St = \frac{2fh}{U} \tag{1}$$

where f denotes the tail beat frequency, and h represents the maximum lateral excursion of the tail end over a cycle. St is used to describe the oscillating mechanism, which serves to judge the flow. Sufficient previous work has shown that animals using oscillatory or waving kinematics configured to operate with a Strouhal number in a narrow range ($0.2 < St < 0.4$) associated with efficient thrust production over a wide range of swimming speed (Taylor et al., 2003; Wolfgang et al., 1999). Fish also tune their kinematics in different constrained flow to produce an optimal wake for maximal hydrodynamic efficiency.

• Dimensionless body wave speed δ (Muller et al., 1997), which is defined as:

$$\delta = \frac{V}{U} \tag{2}$$

It represents the ratio of the body wave speed V to the swimming speeds U; note that live carangiform swimmers always cruise at a δ of slightly greater than 1.

• Dimensionless amplitude h (Hess and Videler, 1984) is defined as:

$$h = \frac{A_{\max}}{L} \tag{3}$$

Received March 30, 2010; revised manuscript received by the editors July 19, 2010. The original version (prior to the final revised manuscript) was presented at the 20th International Offshore and Polar Engineering Conference (ISOPE-2010), Beijing, June 20–25, 2010.

KEY WORDS: Biomimetic robotic fish, self-propelled, efficient swimming, dimensionless parameter, drag reduction.

where A_{max} represents the maximum lateral excursion at the tail end during flapping; the dimensionless amplitude of carangiform fish during steady swimming is normally 0.08~0.12 (Videler, 1993).

Although the relationship between efficient swimming and dimensionless parameters has been widely studied, the corresponding dimensionless parameters of robotic fish with optimal swimming are still unknown. As inherent characteristics of skin friction, body flexibility et al. obviously vary with live carangiform swimmers, it's essential to explore the corresponding relationship between the efficient swimming of man-made undulatory swimmers and the correlative dimensionless kinetic parameters through a special hydrodynamic test. Unfortunately, it is complicated to obtain the quantitative result of thrust efficiency directly. However, some other approaches are worthy of consideration, exploring the parametric dependence of the drag reduction rate, where the drag reduction is defined as P_f/D_uU following Barrett et al. (1999), where P_f is the pure fluid power, D_u is the rigid drag force, and U denotes the self-propelled swimming speed.

Although a variety of different free swimming autonomous robotic fish designs have been produced (Anderson and Chhabra, 2002; Bandyopadhyay, 2005; Kato, 2000; and Long et al., 2006), hydrodynamic experiments for testing drag reduction can only be under taken by the use of the laboratory model that allows specific movement patterns as well as external or internal force measurement. Obviously, a drag reduction experiment can't be conducted using free swimming robotic fish (Lauder et al., 2007). Fig. 1 summarizes 2 main conventional concepts of robotic platforms that are useful for the research of a hydrodynamics experiment. As shown in Fig. 1A, the robotic fish model is attached to a strut which holds the model vertically from the towing carriage above (Bandyopadhyay, 2005; Beal et al,, 2006), or fixed to a place in the water tunnel (Tan et al., 2007); force and torque measurement will be measured by the transducers while the robotic fish model is actively towed at a fixed speed by a towing actuator, or given an oncoming flow velocity. However, the robotic fish is not self-propelled, but moves at a constraint-imposed flow; there is no equality between the thrust and drag force, as indicated by Barrett et al. (1999), and the drag reduction test can only be carried out under conditions of self-propelled mechanism. In Fig. 1B, the robotic fish swims passively on a low-friction bearing guide rail using an undulatory motion, where the thrust force equals the drag force coupled with the strut drag (denoted by D_s) underwater (Morgansen et al., 2001). But the passive towing system has the 2 following defects:

1. An additional part, as shown in Fig. 1 (e.g. slide block, strut, et al.), which cannot be ignored under the force transducer as shown in Fig. 1B (also Fig. 1A); this would result in an increase in the inertia mass of the robotic fish model, consequently, the acceleration of the robotic fish will be different from the real situation.
2. It no longer has the capacity of generating a preset speed for the robotic model, which results in difficulties in measuring the drag force of a rigid model in the water. Taking both active towing system and passive towing system into account, in this paper we propose a novel experimental method which combines the advantages of these 2 methods. Details are presented below.

The remainder of this paper is organized as follows: A brief description of the carangiform robotic fish model and self-propelled experimental system will be introduced first. Then we present the hydrodynamic result of exploring the relationship between dimensionless parameters and the efficient swimming performance of robotic fish. Finally we summarize our research and findings, present the discussions of our work, and the outline for future studies.

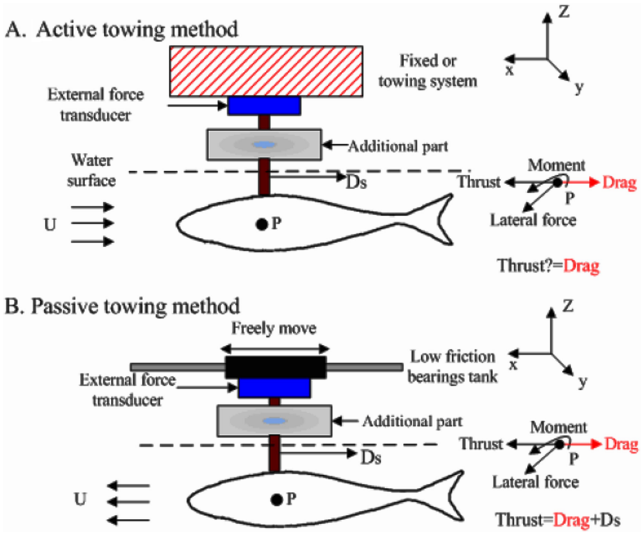

Fig. 1 Schematic view of 2 main conventional categories of flexible fish through hydrodynamic test method

MATERIALS AND METHODS

Experimental Design of Robotic Fish

The robotic fish model has a total length of 0.59 m and consists of a streamlined main body capable of flexing and a rigid propulsive tail fin (Fig. 2). The outer shape of the robotic fish is an exact replica of the shape of a typical carangiform swimmer: Saithe (*Pollachius Virens*), whose body shape parameters have been sufficiently provided. Besides, the mass approximation of robotic fish will ensure the dynamic characteristic. In addition, a great effort was made to imitate the internal mass distribution of the robotic fish body following the real Saithe. The mechanism is a high-precision assembly of 4 links made of anodized aluminum and covered with foams and a special structure, which is made of silica and has a smooth surface so as to reduce friction drag while swimming. Fig. 3A provides details of the outline of the robotic fish, consisting of mechanical links and artificial muscle, as it

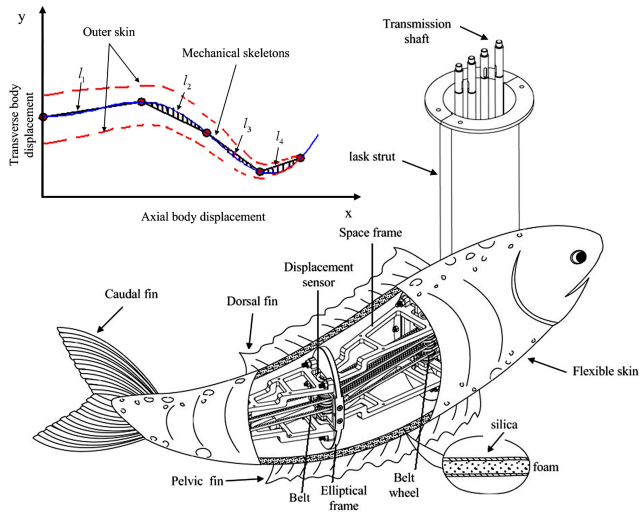

Fig. 2 Schematic view of robotic carangiform swimmer

were, each capable of relative rotation with respect to its neighboring links through activation of the mechanical links driven by 4 brush servo motors (maximum RE 40, 150 W each), which are mounted on a metal plate above water and robotic fish; this occupies the most mass of the additional part mentioned above. All the links are independently controlled by a motion coordinator TRIO MC206, with belts transmitting the motion to individual links with minimal frictional forces, owing to bearings assembled on the shafts (Fig. 3B). Since a waterproof outer skin is used to envelop the whole multilink mechanical skeleton, it is capable of fishlike undulation with the shape of an actual fitting curve. As shown in Fig. 2, relative link lengths were computed to approximate a given smooth, time-varying body-wave curve using geometric optimization.

The undulatory motion is assumed to take the form of a traveling wave, which was also suggested by Lighthill (1970). As mentioned in the Introduction, we do not consider the phase difference between body wave and tail wave, and the tail behaves like an extension of the body wave as previous researchers. predicting the Saithe thrust performance:

$$y(x,t) = (c_1 x + c_2 x^2)\sin(kx \pm \omega t) \tag{1}$$

where the $y(x,t)$ represents the displacement of transverse motion, in a body-fixed coordinate system with x measured starting from the nose of the robotic fish, where $k = 2\pi/\lambda$ is the wave number, corresponding to wavelength λ, while ω is the circular frequency of oscillating, and c_1, c_2 can be adjusted to achieve a specific value for the amplitude envelope for entire body.

Hydrodynamic Test Method of Robotic Fish

Here, we focus on the description of the self-propelled hydrodynamic method, and aim to develop the proper approach so as to explore the relationship between dimensionless parameters and swimming performance of the robotic fish.

Self-propelled experimental method using force feedback. Fishes swim in water by propelling themselves, with their body and tail deforming actively. The mechanism of the self-propelled fish undulate body in the medium is determined by the interaction of fish body movement and unsteady fluid dynamics; the interaction in the forward direction is the result of thrust and drag generated by the body. Currently we just consider the forward direction of fish swimming with the lateral and rotational direction constraint, where this simplified method (e.g. lateral constraint and rotational direction) is widely employed in both experimental and numerical hydrodynamic research of fish swimming while just considering the straight-line swimming.

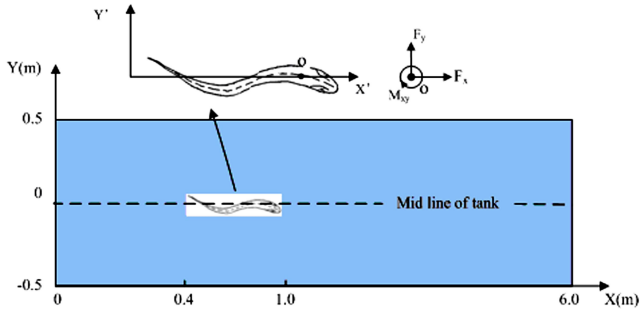

Fig. 3 Carangiform fish swimming in enclosed tank with x, y global coordinates; 0 = center of mass of robotic fish

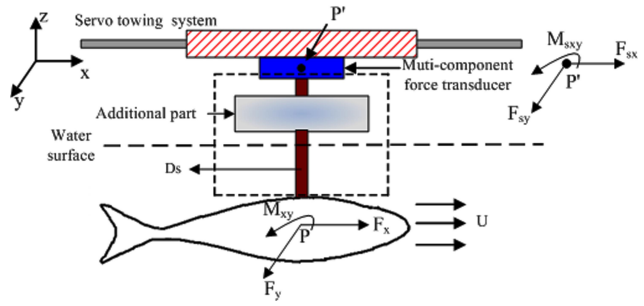

Fig. 4 Schematic view of robotic fish force measurement

The forward translation movement of a free-swimming robotic fish in an enclosed tank (Fig. 3) is determined by the external movement, while the deforming motion is only governed by the internal movement; both internal and external motions are independent of each other. Overall force is regarded as acting on the fish's center of mass. From Newton's law, the force acting on the robotic fish body has to equal the rate of change of momentum of the body as it moves through the water:

$$F_x = ma_x \tag{2}$$

where F_x, F_y, M_{xy} denotes instantaneous force measured by a multicomponent force sensor in the direction of x (forward direction), y (lateral direction) and moment at the center of force sensor P', respectively. m' denotes the mass of the additional parts under the force sensor (apart from the robotic fish mass) as indicated in Fig. 5. The mass of additional parts in our model test includes: The inherent mass of the force sensor, the mass of motor as well as the mechanical transmission system and mass of strut. a'_x represents the acceleration at point P'. As the force sensor is fixed on the towing system, then, a'_x also denotes the acceleration of the towing system derived by the 4,000 W AC motor as shown in Fig. 5.

As Eq. 2 represents the free swimming condition of the robotic fish in the forward direction, and if the acceleration of the towing system a'_x equals the right-hand sides of Eq. 3, the equation can be replaced by Eq. 4, then by Eq. 5 derived:

$$a'_x = \frac{\vec{F}_{sx} + D_s}{m'} \tag{3}$$

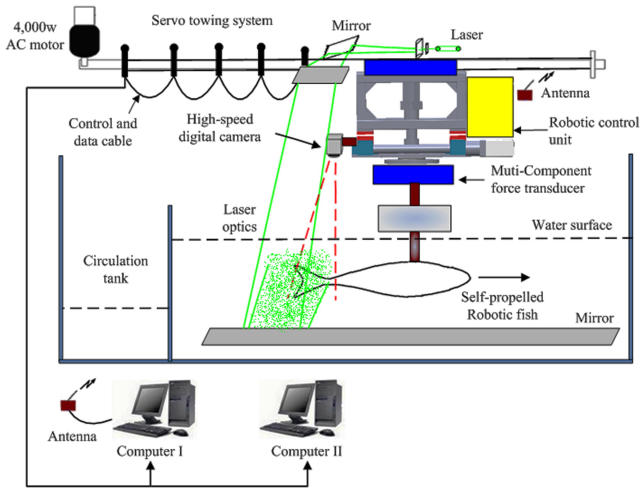

Fig. 5 Schematic view of self-propelled system's experimental system

$$F_x + F_{sx} + D_s = (m + m')\left(\frac{F_{sx} + D_s}{m'}\right) \tag{4}$$

$$F_x = m\left(\frac{\vec{F}_{sx} + D_s}{m'}\right) = ma'_x \tag{5}$$

As F_x denotes the same as in Eq. 2, thus $a'_x = a_x$, the robotic fish fixed in a towing system will satisfy the free swimming (e.g. self-propelled) in the forward direction according to Eq. 3. When the robotic fish undulates its body in water, the instantaneous force and moment signal will be measured by the force sensor, and force-feedback control will be carried out. To relate the force to kinematics, we represent the motion of the fish center of mass in the forward direction, defined as Eq. 6, then replaced by the time-discrete form as shown in Eq. 7:

$$v'_x = \int_0^t \left(\frac{F_{sx} + D_s}{m'}\right) dt \tag{6}$$

$$U_x(t) = \sum_{i=1}^{n} \left(\frac{F_{sx} + D_s}{m'}\right) \Delta t \tag{7}$$

Eq. 7 is now to govern the forward speed $U_x(t)$ expressed as a time-discrete form with the force feedback by the sensor. Even a small change in F_{sx} will be fed back, corresponding the change in forward speed U_x. The lateral force F_{sy} and the moment M_{sxy} can also be measured simultaneously while the towing system completes the forward free swimming.

To implement such a complicated instrument, as shown in Fig. 6, the robotic fish is mounted vertically under the Kistler quartz crystal 3-component sensors 9254C, which has a natural frequency of 3 kHz, high rigidity of 500 N/μm, and sensitivity of 0.005 N in the forward direction. The fish's center of mass is vertically below the center of the Kistler, the robotic fish model together with Kistler and accurately fixed on the towing system which is provided by German Schneider. As noted above, lateral force F_{sy} and moment M_{sxy} can be measured simultaneously by this sensor. The water tank has these dimensions: 7.8 m × 1.2 m × 1.1 m; the circulation tank is 2-m long in the forward direction. The output of the robotic fish internal force as well as the external force measured by the Kistler are recorded in computer I (Fig. 5) through a connecting cable using CAN bus; simultaneously, the forward force F_{sx} will be transmitted to the motion coordinator Trio MC206 for acceleration control via Eq. 5. The particle image will be transferred through another cable to computer II for flow visualization analysis, while the laser sheet will pass through the middle of the robotic fish caudal fin. A high-speed CCD camera covered by an optical band pass filter was used to capture the particle image.

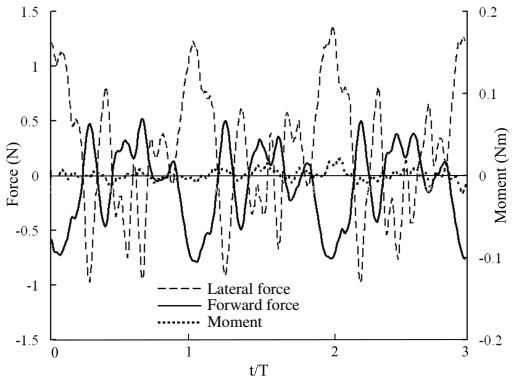

(A)

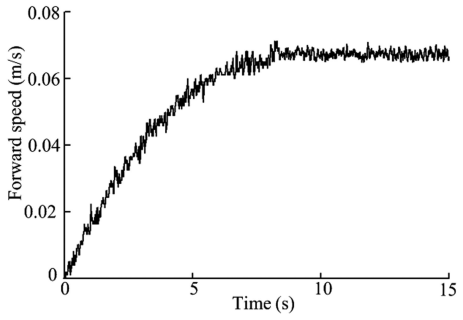

(B)

Fig. 6 A. Lateral force (dashed line), forward force (drawn line), total moment at fish center of mass (dotted line); B. forward speed of robotic fish under self-propelled condition

As described above, the internal and external force measurement as well as PIV visualization can be implemented simultaneously under the self-propelled condition. As an example, Fig. 6 shows the measured external force (Fig. 6A) associated with the forward velocity U_x (Fig. 6B) of robotic fish over several cycles of undulatory movement under the self-propelled condition, for the following kinetic parametric value: the dimensionless tail end amplitude $h = 0.1$; flapping frequency of $f = 0.6$ Hz; the $\lambda = 0.8$.

Description of efficient swimming of robotic fish using drag rate. To make robotic fish swimming efficient, we must understand the thrust efficiency; however, it is impossible to distinguish the fish's body and tail, as both provide thrust and drag at the same time. This point had also been indicated by previous researchers. As mentioned in the Introduction, the drag reduction rate is closely related to efficient swimming performance of the robotic fish; it is also an integrated embodiment of the forward thrust force and drag. Here, we choose to explore the optimum swimming pattern of robotic fish by studying the parametric dependence of the observed drag reduction rate on the dimensionless parameters *St,* δ and h.

By conservation of net power supplied by the robotic fish, P_p denotes the total time-averaged power expended by the motors (Eq. 8) to drive the mechanical links which can be further written as the sum of useful power P_E, and power loss P_l, which denotes the mechanical transmission losses from the motors to the fish's mechanical links; P_w denotes the energy wasted in the flow and wakes:

$$P_p = P_E + P_l + P_w \tag{8}$$

Here we define drag rate as follows:

$$I_p = \frac{P_p - P_l}{D_u U} = \frac{P_f}{D_u U} \tag{9}$$

where D_u represents rigid body drag at a given speed U. When $I_p < 1$, drag reduction happens, as indicated by Barrett et al. (1999). Note that the power here refers to that consumed purely in fluid denoted as P_f in Eq. 9. Although considerable effort was expended trying to minimize force losses in the belt-wheel transmitting mechanism, the measured force in water includes not only the unsteady hydrodynamic fluid force but also internal mechanism force losses, and the preload of belt force of the measurement system.

The most significant difference between the current self-propelled method and Barrett's (1999) is that the total number of experimental runs decreased a lot. Over 600 experiments were

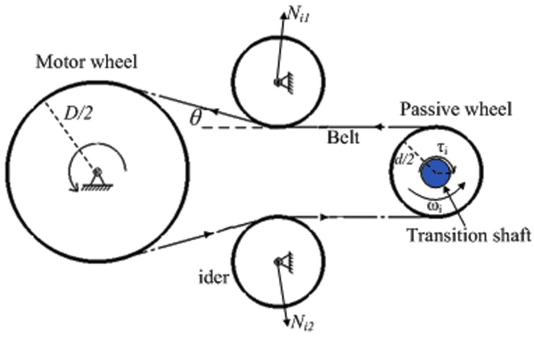

Fig. 7 Schematic view of internal torque measurement system for each mechanical link; dashed line = belt

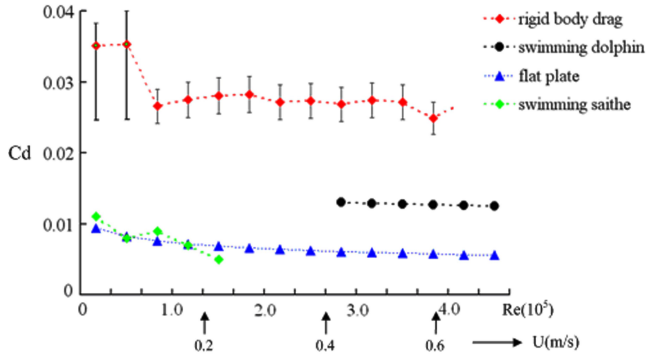

Fig. 8 Drag coefficient versus flow speed and corresponding Reynolds number

conducted on robotic tuna at fixed flow speed, but for a self-propelled body the drag force must equal the thrust force; most experimental runs do not satisfy this condition and were abandoned, while in current experiments every single run is self-propelled.

Power consumption measurement of robotic fish. We obtained the internal power by measuring the instantaneous belt tension. (Dynamic torque sensor was not used because of its larger space and mass.) Belts are connected to each motor wheel; each wheel is connected to the motor output axis, and drives the passive wheel by the belt. For the i-th motor corresponding to the i-th mechanical link, the upside belt is pulled in while registering force N_{i1}, and the downside is paid out while registering force N_{i2} (Fig. 7), while the idler presses the outside of the synchronous belt firmly. By mounting the pressure sensor on the idler, N_{i1} and N_{i2} can be measured. The relations of N_{i1}, N_{i2} and the torque M_i are strictly deduced as follows; the deduction process is not shown:

$$M_i = \left(\frac{N_{i1}}{(1+e^{2r\theta}) \cdot \sin\theta} - \frac{N_{i2}}{(1+e^{-2r\theta}) \cdot \sin\theta} \right) \cdot \frac{d}{2} \tag{10}$$

where r denotes the friction coefficient between belt and idler ($r = 0.29166$); θ represents the wrap angle of the transmission belt on the idler; d is the diameter of the passive wheel. In the process of measuring, we chose 8 pressure sensors and calibrated by hanging various weights. Linearity was better than 0.5%; while repeated every 3 days over a period of one month, test results provided consistent constants with no apparent drift (long-term variations of about 1%). The pressure sensor signal is transmitted by CAN bus and finally is sent to Computer I for analysis (Fig. 5).

The instantaneous power is obtained as $P_j = M_j \omega_j$, where the ω_j denotes the angular speed of each motor. The overall instantaneous power is calculated as the sum of the input power in all joints and integrated to find the average power, which is represented by P (Eq. 11) after self-propelled steady swimming is achieved. In the experiment, a dynamic measurement calibration method was used in order to ensure the power consumption measurement's precision, and the result of the final dynamic power consumption calibration shows that the power consumption error is within 5%; the total power consumption of the fish body within a period can be expressed as:

$$P = \frac{\int_0^T \sum_{i=1}^{i=4} M_i(t)\omega_i(t)dt}{T} \tag{11}$$

HYDRODYNAMIC RESULTS

An important dimensional parameter of carangiform swimmers is the Reynolds number, which is defined as:

$$Re = UL/v \tag{12}$$

where L denotes fish length, U represents the steady swimming speed under the self-propelled condition, v denotes the kinematic viscosity of the water. Our robotic carangiform swimmer typically achieves high Reynolds number $Re > 10^4$, well within the so-called inertial regime; the viscous forces are negligible and inertial forces dominate the dynamics of motion.

The robotic fish have a submergence of 0.25 m (lateral line of rigid body) to minimize interference with the free surface and the bottom of the tank. We first conducted the force measurement of rigid body drag, but the testing result of the external force measured by Kistler contains the drag of the strut including some wave-making drag at the free surface, the interaction drag among the fish body, the strut and the rigid fish body. As shown in Eq. 11, only the rigid body drag D_u is needed for our drag rate test; the remaining components must be measured and subtracted. For this reason, we measured experimentally, as a function of active towing speed U, which ranges from 0 to 0.7 m/s at small increments of 0.05 m/s: The strut drag had the fish body removed and thus we obtained the net drag on the robotic fish body. Each run was conducted 3 times to ensure the repeatability and accuracy of the test result; over 50 experimental runs were done during the drag test.

For ease of comparison with previous researchers' experimental results, the corresponding rigid body's drag coefficient based on the wetted area A_w is defined in Eq. 13:

$$C_d = D_u / 0.5\rho A_w U^2 \tag{13}$$

where ρ denotes the water density, and A_w represents the wetted area of the robotic fish body; Fig. 9 provides the rigid body drag coefficient, as well as the flat-plate (with a length-to-diameter ratio of 5.0) drag in turbulent flow provided by Hoerner (1965), the body drag coefficient of bottom-nosed dolphins provided by Fish (1993), and Saithe provided by Videler (1993). The result shows that the final drag coefficient measured in the experiment is between 0.025 and 0.04, slightly decreased with the increase of the Re number. Although the length-to-diameter ratio of the fish body is 1/6 and smooth silicon material was used as the artificial skin of the robotic fish, its drag coefficient is much greater than that of a real carangiform swimmer, even with the same body shape. According to the analysis, we found the main cause is that

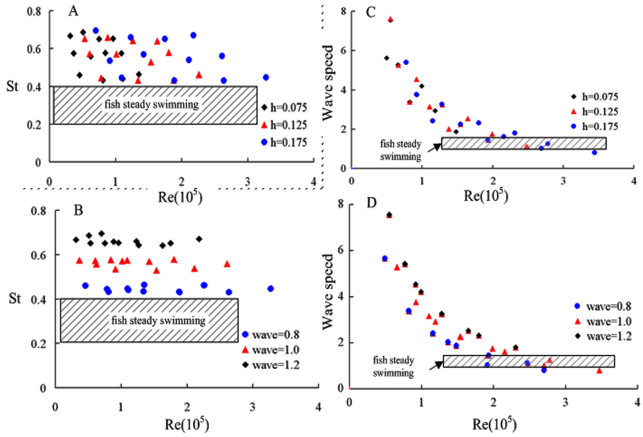

Fig. 9 A: *St* of robotic fish as a function of *Re* number for different dimensionless tail-end amplitude. B: *St* as a function of *Re* for various wavelength value C: Wave speed δ as a function of *Re* for different h. D: Wave speed δ as a function of *Re* for different dimensionless wavelength.

the surface of the robotic fish became slightly rugged under the function of water pressure, although various methods has been adopted. It should be noted that under the condition of a very low *Re* number (less than the towing speed of 0.05 m/s), it's complicated to acquire accurate data as the drag force is so small (< 0.005 N) and beyond the capacity of Kistler.

Efficient swimming sensitivity to dimensionless parameter. To systematically quantify the effect of dimensionless parameters on the drag rate of carangiform robotic fish, it was decided to perform systematic tests at a number of fixed undulatory frequency: $f =$ 0.6, 1.0, 1.4 and 1.8 Hz. At each value of frequency, the tests are performed for a number of fixed wavelength: $\lambda = 0.8, 1.0, 1.2$. For each combination of f and λ, the dimensionless heave amplitude was set as $h = 0.075, 0.125, 0.175$. First, we will analyze the test result of robotic fish swimming under the self-propelled condition.

Fig. 9A shows the 2 dimensionless parameter: the Strouhal number and wave speed of robotic fish swimming under the self-propelled condition as a function of *Re* number for several kinematics parametric value of h and dimensionless wavelength (denoted as *wave* for short in Figs. 9B and D). The *St* range of robotic fish swimming is 0.41∼0.72, and shows no tendency to vary with the *Re* number obviously or regionally, while this phenomenon is similar to the biological observation result. Fig. 9B shows *St* gradually deviating from the fish steady swimming region ($0.2 < St < 0.4$) with increasing body wavelength. As noted in the Introduction, the steady cruising wave speed of an undulatory swimmer is normally greater than 1 and from 1.1 to 1.3, which is represented by the shadow area in Fig. 9C and D. Under the condition of $Re > 2 \times 10^5$ (i.e. steady swimming speed $U > 0.3$ m/s), the wave speed of robotic fish δ gradually converged between 1.0 and 1.2 and approximates the range of live swimmers.

We provide detailed measurement data for 2 typical cases, which are closest to the observed dimensionless experimental data of real fish for further analysis. From Table 1, both cases provide *St* and wave speed approximate to the result of a live Saithe. Meanwhile, the difference of *St* between the 2 cases is tiny, and the wave speed is within the range of efficient fish steady swimming. It should be noted that Case 2 also corresponds to the maximum swimming speed of robotic fish at a speed of 0.98 *BL*/s (i.e. 0.588 m/s). While Case 3 provides a result of the lowest *St* number among all experimental data, the corresponding wave speed of Case 3 is 2.03, obviously larger than the biological observation result.

Variable	Abbreviation	Case 1	Case 2	Case 3	Saithe
Reynolds number (10^5)	*Re*	2.47	3.35	2.68	2∼8
Speed (U/L)	*U*	0.71	0.98	0.77	1.4
Wave length	λ	0.8	0.8	0.8	1.04
Tail end amplitude	h	0.125	0.175	0.175	0.083
Wave speed	δ	1.119	1.034	2.034	1.20
Strouhal number	*St*	0.426	0.422	0.41	0.34

Table 1 Comparison of kinematics result between robotic fish and live swimmer

Compared with the *St* of a cruising Saithe, the minimal *St* value of robotic fish under self-propelled conditions is higher than that of a live swimmer ($St = 0.34$). The biological estimating result indicates that when the $St > 0.3$, the swimming efficiency of fish will gradually decrease with the *St* number increase. We may hypothesize that the swimming efficiency of live fish should be higher than current robotic fish based on the above evidence.

Barrett et al. (1999) concluded that the undulate motion is drag-reducing since the bound drag estimate was found to be less than that of the corresponding rigid body drag under the condition of fixed *Re* ($Re = 7 \times 10^5$), and at fixed towing speed $U = 0.7$ m/s. Fig. 10 shows the parametric dependence of the observed drag rate I_p on the principal dimensionless parameters, while Fig. 10A shows the drag rate decreased and converged gradually with the *Re* number increase (i.e. increasing swimming speed), and the value of the *Re* number greater than 2.4×10^5 provides drag reduction, Fig. 10B showed a relatively small experimental set of drag rate (where $I_p < 2$), where a narrow range of Strouhal number $0.41 < St < 0.43$ is found to provide all drag reduction cases, with a peak at $St = 0.422$; it can also be found that the value of body wave speed δ in the range of 1 to 1.5 ($1 < \delta < 1.5$) provides all drag reduction cases, so it is clearly shown that drag reduction did not occur in other ranges.

Fig. 10D provides a comparison between the 2 cases corresponding to minimal drag rate and some classic results done by

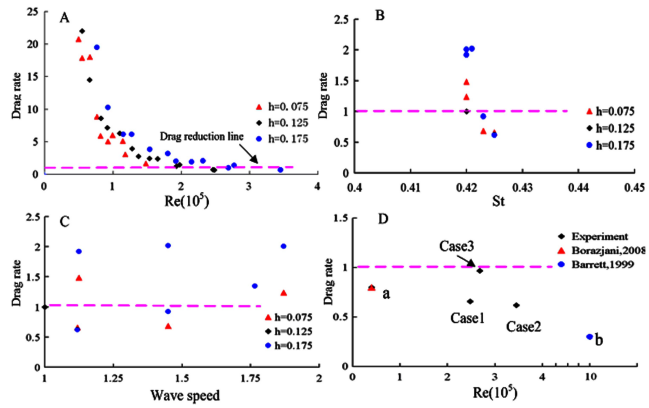

Fig. 10 Pink-dotted line = drag reduction line, where $I_p = 1$. A: experimental result of *Re* versus drag rate. B: *St* versus drag rate while at $I_p < 2$. C: Body wave speed versus drag rate at $I_p < 2$ and D: comparation with previous researchers' result.

Variable	Abbre-viation	Case 1	Case 2	Case 3	a	b
Strouhal number	St	0.426	0.422	0.41	0.3	0.25
Drag coefficient	C_d	0.024	0.02	0.026	—	0.012
Mechanical power (W)	P_l	0.029	0.082	0.0638	—	0.492
Fluid power	P_f	0.0653	0.168	0.106	—	0.588
Drag rate	I_p	0.688	0.62	0.978	0.85	0.5

Table 2 Variables for hydrodynamic quantities and compared result

previous researchers.. Table 1 shows the experimental result of Barrett's robotic tuna (Barrett et al., 1999), which indicates that at fixed $Re = 10^6$, a maximal drag reduction of 50% is provided. (Note that the maximum drag reduction rate realized on robotic tuna for the self-propelled motion is not the well-known value 70%, but 50%.) Borazjani et al. (2008) provided a drag reduction of 15% at a Strouhal number of 0.34 under the condition of $Re = 0.04 \times 10^5$, while in the current test we obtain a maximal drag reduction rate of 38% at $Re = 3.35 \times 10^5$. By comparing Case 1 to Case 3 (Table 2), although Case 3 provides a peak swimming St among all experimental data, its corresponding wave speed ($\delta = 2.03$) is much greater than that of live swimmers; consequently, the result is a drag rate of 0.978, where less drag reduction rate is performed than that in Cased 1 and 2.

And in all cases where substantial drag reduction happened in our experiment, the wave speed of robotic fish exceeded the swimming velocity U, in complete agreement with 3D plates' simulation result of 3D waving plate. The power consumed purely in fluid is quite small and does not exceed 1 Watt in the current experiment. According to Table 2, the mechanical transmission loss came at 45% of the total power loss using steel wire to drive the fish body, compared to current robotic fish, which reduced to 32% by use of belt transmission.

The most important findings that follow from Figs. 9 and 10 as well as the above descriptions can be summarized as follows:

• The maximal drag reduction rate (38%) is observed for parametric value where St and δ are proximal dimensionless parameters of live undulatory swimmers' efficient swimming.

• Drag reduction increases slightly with Re number; this may be of great significance for robotic fish while at greater cruising speed or larger scale. This result is in agreement with the conclusions of Borazjani et al. (2008) and Barrett et al. (1999).

• Efficient swimming of robotic fish is not solely dependent on St; other dimensionless parameters should be also within optimal range associate with St, where St is around 0.42, and δ lies between 1.0 and 1.2.

It's not surprising to find that low drag rate (i.e. high drag reduction) is observed for parametric values where the St number is close to the efficient thrust production of natural creatures, for the Strouhal number, which governs the dynamics of shed vorticity and waving motion, is a principal parameter in undulatory swimming (Anderson et al., 1998). As the quantitative thrust efficiency of robotic fish cannot be obtained directly by hydrodynamic experiment, systematical research on the effect of dimensionless parameters on the drag rate is an effective approach with which to understand the efficient swimming pattern of robotic fish. In the current research, we employed self-propelled methods to make the robotic fish experimentally learn to swim efficiently, and finally we obtained the optimal St number of around 0.42 for robotic fish, and another dimensionless parameter wave speed within the optimal range of 1.0∼1.2. Efficient swimming of robotic fish in different swimming speed requires the Strouhal number primarily, and other parameters of the undulatory body to a somewhat lesser degree (here we use wave speed and dimensionless amplitude) must be within optimal, relatively narrow ranges.

DISCUSSION

In this paper, we present a novel experimental method to conduct force and power measurement on a robotic fish which mimics a live carangiform swimmer. The present hydrodynamic experiment differs from previous work in that the forward swimming speed of the robotic fish is not specified, but obtained by force feedback calculation. The systematic test results showed a maximum drag reduction rate of 38% under the self-propelled condition. This is obtained at Reynolds number 3.34×10^5, and is observed for parametric value where the Stouhal number and dimensionless wavespeed are proximal to those of live undulatory swimmers. This is also the most important findings of the current experiment. Systematic flow analysis of the robotic fish wake structure will be carried out on the self-propelled towing system in the near future.

Although currently the body and tail of robotic fish are treated together as a single undulatory wave for simplicity, as Hess and Videler (1984) do, recent findings show that the caudal fin undergoes complex kinematics independent of body in some scombrid fishes (e.g., mackerel, tuna), thus shedding vorticity in different way. Considering this, more principal parameters besides current dimensionless parameters will be taken into consideration to explore better swimming performance for a robotic fish.

ACKNOWLEDGEMENTS

Many thanks to Prof. George V. Lauder for his kind suggestion to this research. Also, I was very grateful to Li Jinlan and Fan Zhe for their assistance during the hydrodynamic experiment in the wet, hot basement. This work was supported by National Outstanding Youth Science Foundation support projects, China, under contract # 60525314.

REFERENCES

Anderson, JM, Streitlien, K, Barrett, DS, and Triantafyllou, MS (1998). "Oscillating Foils of High Propulsive Efficiency," *J Fluid Mech*, Vol 360, pp 41–72.

Anderson, JM, and Chhabra, N (2002). "Maneuvering and Stability Performance of a Robotic Tuna," *Integr Computat Biol*, Vol 42, pp 118–126.

Bandyopadhyay, PR (2005). "Trends in Biorobotic Autonomous Undersea Vehicles," *IEEE J Oceanic Eng*, Vol 30, pp 109–139.

Barrett, D, Triantafyllou, M, Yue, D, Grosenbaugh, M, and Wolfgang, M (1999). "Drag Reduction in Fish-like Locomotion," *J Fluid Mech*, Vol 392, pp 183–212.

Beal, DN, Hover, FS, Triantafyllou, MS, Liao, J, and Lauder, GV (2006). "Passive Propulsion in Vortex Wakes," *J Fluid Mech*, pp 385–402.

Borazjani, I (2008). "Numerical Investigation of the Hydrodynamics of Carangiform Swimming in the Transitional and Inertial Flow Regimes," *J Exp Biol*, Vol 212, pp 576–592.

Cheng, J-Y (1994). "Note on the Calculation of Propeller Efficiency Using Elongated Body," *J Exp Biol*, Vol 192, pp 169–177.

Fish, FE (1993). "Power Output and Propulsion Efficiency of Swimming Bottlenose Dolphin," *J Exp Biol,* Vol 185, pp 179–193.

Hess, F, and Videler, JJ (1984). "Fast Continuous Swimming of Saithe (*Pollachius virens*): A Dynamic Analysis of Bending Moments and Muscle Power," *J Exp Biol*, Vol 109, pp 229–251.

Hoerner, SF (1965). *Fluid-Dynamic Lift*, Hoerner Fluid Dynamics.

Kato, K (2000). "Control Performance in the Horizontal Plane of a Fish Robot with Mechanical Pectoral Fins," *IEEE J Oceanic Eng*, Vol 25, pp 121–129.

Lauder, GV, Anderson, EJ, Tangorra, J, and Madden, PGA (2007). "Fish Biorobotics: Kinematics and Hydrodynamics of Self-Propulsion," *J Exp. Biol*, Vol 210, pp 2767–2780.

Lauder, GV, and Drucker, EG (2002). "Forces, Fishes, and Fluids: Hydrodynamic Mechanisms of Aquatic Locomotion," *News Physiol Sci*, Vol 17, pp 235–240.

Lighthill, MJ (1960). "Note on the Swimming of Slender Fish," *J Fluid Mech*, Vol 9, No 2, pp 305–317.

Lighthill, MJ (1970). "Aquatic Animal Propulsion of High Hydrodynamic Efficiency," *J Fluid Mech*, Vol 44, pp 265–301.

Long, JH, et al. (2006). "Biomimetic Evolutionary Analysis: Testing the Adaptive Value of Vertebrate Tail Stiffness in Autonomous Swimming Robots," *J Exp Biol*, Vol 209, pp 4732–4746.

Morgansen, K, Duindam, V, Mason, R, Burdick, J, and Murray, R (2001). "Nonlinear Control Methods for Planar Carangiform Robot Fish Locomotion," *Proc IEEE Int Con. Robot Automation.*, pp 427–434.

Muller, UK, Van den Heuvel, B, Stamhuis, EJ, and Videler, JJ (1997). "Fish Footprints: Morphology and Energetic of the wake behind a Continuously Swimming Mullet (Chelon labrosus Risso)," *J Exp Biol*, Vol 200, pp 2893–906.

Muller, UK, Stamhuis, EJ, and Videler, JJ (2000). "Hydrodynamics of Unsteady Fish Swimming and the Effects of Body Size: Comparing the Flow Fields of Fish Larvae and Adults," *J Exp Biol*, Vol 203, pp 193–206.

Muller, UK, Smit, J, Stamhuis, EJ, and Videler J (2001). "How the Body Contributes to the Wake in Undulatory Fish Swimming: Flow Fields of a Swimming Eel (Anguilla)," *J Exp Biol*, Vol 204, pp 2751–2762.

Nauen, JC, and Lauder, GV (2002). "Hydrodynamics of Caudal Fin Locomotion by Chub Mackerel," *J Exp Biol*, Vol 205, pp 1709–1724.

Rohr, JJ, and Fish, FE (2004). "Strouhal Numbers and Optimization of Swimming by Odontocete Cetaceans," *J Exp Biol,* Vol 207, pp 1633–42.

Sfakiotakis, M, Lane, DM, and Davies, JBC (1999). "Review of Fish Swimming Modes for Aquatic Locomotion," *IEEE J Oceanic Eng*, Vol 24, No 2, pp 237–252.

Tan, Guang-Kun, Shen, Gong-Xin, and Huang, Shuo-Qiao (2007). "Investigation of Flow Mechanism of a Robot Fish Swimming by Utilizing Flow Visualization Synchronized with Hydrodynamic Force Measurement," *Experiments in Fluids*, Vol 43, pp 811–821.

Taneda, S, and Tomonari, Y (1974). "An Experiment on the Flow Around a Waving Plate," *J Phys Soc*, Vol 36, pp 1683–1689.

Taylor, G.K, Nudds, RL, and Thomas, ALR (2003). "Flying and Swimming Animals Cruise at a Strouhal Number Tuned for High Power Efficiency," *Nature*, Vol 425, pp 707–711.

Triantafyllou, MS, Triantafyllou, GS, and Yue, DKP (2000). "Hydrodynamics of Fish Swimming," *Annul Rev Fluid Mech*, Vol 32, pp 33–53.

Triantafyllou, GS, Triantafyllou, MS, and Grosenbaugh M (1993). "Optimal Thrust Development in Oscillating Foils with Application to Fish Propulsion," *J Fluids Struct*, Vol 7, pp 205–224.

Tytell, ED, and Lauder, GV (2004). "The Hydrodynamics of Eel Swimming—I: Wake Structure," *J Exp Biol*, Vol 207, pp 1825–1841.

Videler, JJ (1993). *Fish Swimming*. London: Chapman & Hall.

Wolfgang, MJ, et al. (1999). "Near-Body Flow Dynamics in Swimming Fish.," *J Exp Biol,*" Vol 202, pp 2303–2327.